LETTER

https://doi.org/10.1038/s41586-019-1574-8

Kimberlites reveal 2.5-billion-year evolution of a deep, isolated mantle reservoir

Jon Woodhead[1]*, Janet Hergt[1], Andrea Giuliani[1,2,5], Roland Maas[1], David Phillips[1], D. Graham Pearson[3] & Geoff Nowell[4]

The widely accepted paradigm of Earth's geochemical evolution states that the successive extraction of melts from the mantle over the past 4.5 billion years formed the continental crust, and produced at least one complementary melt-depleted reservoir that is now recognized as the upper-mantle source of mid-ocean-ridge basalts[1]. However, geochemical modelling and the occurrence of high $^{3}He/^{4}He$ (that is, primordial) signatures in some volcanic rocks suggest that volumes of relatively undifferentiated mantle may reside in deeper, isolated regions[2]. Some basalts from large igneous provinces may provide temporally restricted glimpses of the most primitive parts of the mantle[3,4], but key questions regarding the longevity of such sources on planetary timescales—and whether any survive today—remain unresolved. Kimberlites, small-volume volcanic rocks that are the source of most diamonds, offer rare insights into aspects of the composition of the Earth's deep mantle. The radiogenic isotope ratios of kimberlites of different ages enable us to map the evolution of this domain through time. Here we show that globally distributed kimberlites originate from a single homogeneous reservoir with an isotopic composition that is indicative of a uniform and pristine mantle source, which evolved in isolation over at least 2.5 billion years of Earth history—to our knowledge, the only such reservoir that has been identified to date. Around 200 million years ago, extensive volumes of the same source were perturbed, probably as a result of contamination by exogenic material. The distribution of affected kimberlites suggests that this event may be related to subduction along the margin of the Pangaea supercontinent. These results reveal a long-lived and globally extensive mantle reservoir that underwent subsequent disruption, possibly heralding a marked change to large-scale mantle-mixing regimes. These processes may explain why uncontaminated primordial mantle is so difficult to identify in recent mantle-derived melts.

Kimberlites, a group of volatile-rich silica-poor magmas, represent the only melts that are known to sample the deep mantle of the Earth. Diamonds that have been brought to the surface in some kimberlite eruptions contain inclusions of minerals that can only derive from great depth, such as majoritic garnet and ringwoodite from the transition zone[5], and magnesium perovskite and calcium perovskite (which derive at least from the boundary between the upper and lower mantle, and possibly from up to 800 km deep)[6]. Consequently, some—if not all—kimberlites are likely to have originated from at least this depth[7]. Kimberlitic magmas have been erupting on Earth for at least 2.85 billion years (Gyr)[8], and thus offer a unique window into the chemical evolution of deep-mantle regions across much of the Earth's history. This view is not available from ocean island basalts (which are frequently used as probes of the compositions of present-day mantle) owing to the relative youth of the ocean basins in which they occur, or from large igneous provinces, which are temporally and spatially restricted. We compiled new and existing neodymium- and hafnium-isotope data for globally distributed kimberlites; our data encompass samples with well determined eruption ages that span more than 2 Gyr (Supplementary Data). Where possible, we restrict our study to samples that are petrographically and mineralogically equivalent to archetypal kimberlites, and have filtered the dataset to exclude samples that may have experienced substantial crustal assimilation (Methods).

Our compilation reveals that—before about 200 million years ago (Ma)—the mantle source of all kimberlite bodies globally appears to have evolved along a single isotopic trajectory over more than 2 Gyr of the Earth's history (through the Proterozoic eon). This indicates that these bodies derived from a relatively homogeneous source that had a composition very close to that of the chondritic uniform reservoir (CHUR) model[9] for the Earth's primitive mantle (Fig. 1). We term this group the 'primitive' kimberlites. To place this observation in perspective, the narrow isotopic variation that is recorded in kimberlites across the globe throughout this period is comparable to that observed in the modern mid-ocean-ridge basalt (MORB) source[10] (Fig. 2a) and at least half of this variability (four to five epsilon units) can be accounted for through simple radiogenic ingrowth during this time. For an assumed deep-mantle reservoir of such homogeneity and global extent to have been maintained for close to half the age of the Earth (and probably more), a source that is both ancient and that has remained isolated from the depleted, convective upper mantle for the majority of this time is required. Figure 2b shows that the integrity of this domain is unlikely to have been maintained if substantial contamination by subducted components had occurred. The fact that kimberlite magmas originate in the deeper mantle and have tapped a homogeneous source that is compositionally distinct from the depleted MORB mantle (DMM) over a very long period of time raises the possibility that this source—of worldwide extent—may represent a primordial-mantle composition that has remained isolated for billions of years.

Although most kimberlites younger than 200 million years (Myr) old continue to evolve along the same primitive trajectory, samples from at least three large kimberlite fields generated after 200 Ma (in southern Africa, Brazil and western Canada) appear to define separate steeply inclined trajectories in neodymium- and hafnium-isotope space. We term these 'anomalous' kimberlites (Fig. 3). The origin of these steeper arrays is considered below: however, it is important to note here that—in all three areas—older samples (from before the Mesozoic era) plot along the primitive trend, whereas kimberlites younger than 200 Myr old from the same areas experienced a distinct chemical perturbation that produced a sudden and marked decrease in the $^{143}Nd/^{144}Nd$ and $^{176}Hf/^{177}Hf$ ratios of their source.

The potential preservation of portions of the Earth's primitive mantle, and its likely composition, continue to be debated[3,11–13]. Although it has recently been demonstrated that the bulk Earth originally had a genetic evolution that is similar to that of enstatite chondrites[14], the critical question of whether any pristine primordial reservoirs still exist is difficult to address. This is largely because our evidence is provided by isolated sample suites (such as the approximately 60-Myr-old picrites of Baffin Island[3]) that provide snapshots in time, which may only by coincidence correspond to a predicted primitive-mantle composition at a given point in the Earth's history. Kimberlite data offer a different

[1]School of Earth Sciences, University of Melbourne, Melbourne, Victoria, Australia. [2]Department of Earth and Planetary Sciences, Macquarie University, Sydney, New South Wales, Australia. [3]Department of Earth and Atmospheric Sciences, University of Alberta, Edmonton, Alberta, Canada. [4]Department of Earth Sciences, Durham University, Durham, UK. [5]Present address: Institute of Geochemistry and Petrology, Department of Earth Sciences, ETH Zurich, Zurich, Switzerland. *e-mail: jdwood@unimelb.edu.au

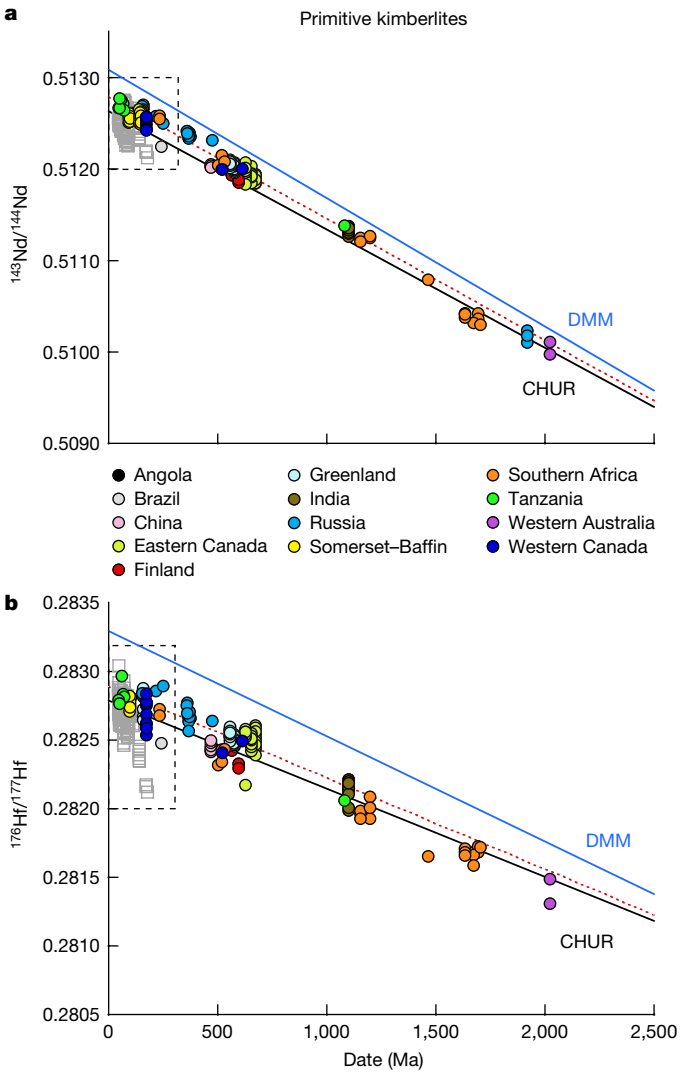

Fig. 1 | Isotopic evolution in the global kimberlite dataset. a, **b**, Plots of neodymium (**a**) and hafnium (**b**) isotopic evolution over time reveal two distinct evolutionary trajectories. All kimberlites formed before about 200 Ma (and some formed thereafter) appear to be derived from a single, relatively homogeneous source: the primitive kimberlites, denoted by coloured circles. At around 200 Ma, a major disruption is observed in three regions (grey squares), which subsequently exhibit a very different isotopic character. The evolutionary trends for DMM, the CHUR model and a linear regression through the primitive-kimberlite data anchored to the CHUR model at 4.55 Ga (red dotted line) are also shown. Regions in dashed boxes in **a** and **b** are shown in Fig. 3a and Fig. 3b, respectively.

perspective on this issue. At the most fundamental level, any surviving remnant of an early primordial reservoir must be demonstrably very long-lived, relatively homogeneous, compositionally distinct from the bulk of the convecting upper mantle (DMM) and conform to an estimate of a primordial composition[15]. The mantle source of the primitive group of kimberlite magmas noted above is perhaps the only reservoir on Earth yet identified that satisfies all of these requirements. The isotope ratio and age data reveal the long-term evolution of a relatively homogeneous deep-mantle source that is isotopically distinct from DMM (Figs. 1, 2), and that has seemingly remained isolated from substantial sediment recycling for about 2 Gyr. Furthermore, the isotopic evolution of this source with time appears to be very close to our best estimate of a primitive-mantle composition (the CHUR model). Using best-fit lines through the arrays in Fig. 1, anchored to a CHUR isotopic composition at 4.55 Gyr ago (Ga), we can estimate the present-day isotopic composition of this reservoir (a $^{143}Nd/^{144}Nd$ ratio of 0.512783 and a $^{176}Hf/^{177}Hf$ ratio of 0.282886) and the parent/daughter-isotope ratios implied by the isotopic evolution of the reservoir (a $^{147}Sm/^{144}Nd$ ratio of 0.2011 and a $^{176}Lu/^{177}Hf$ ratio of 0.0347). These parent/daughter-isotope ratios appear slightly super-chondritic when compared with the reference values for CHUR[15] of 0.1960 and 0.0336, respectively, but it is clear that their scatter encompasses the CHUR evolution line.

Other geochemical data provide corroborating evidence. For example, ratios of the less-mobile trace elements (particularly Nb/Ta, 19 ± 5, ± 1 s.d., and Nb/Th, 11 ± 5, ± 1 s.d.) in samples from the primitive-kimberlite dataset are within the uncertainty of primitive-mantle values (17.7 and 8.3, respectively)[16] and distinct from DMM values (15.5 and 18.8, respectively)[17]. Other elemental ratios such as La/Nb and Ba/Nb also readily distinguish primitive-mantle reservoirs (1 and 10, respectively)[16] from the DMM (1.3 and 3.8, respectively)[17] and crustal sources (2.2 and 52, respectively)[18]. Despite the greater scatter in Ba/Nb relative to La/Nb ratios, due to potential secondary Ba mobility, the means of both these ratios in the kimberlites ($La/Nb = 0.8 \pm 0.4$, ± 1 s.d., and $Ba/Nb = 10 \pm 10$, ± 1 s.d.) are similar to estimates of primitive mantle. The suggestion that the kimberlites may track a primordial source is also supported by helium isotope systematics: $^{3}He/^{4}He$ ratios of up to $27\times$ the atmospheric value (R_A) in samples of fresh kimberlitic olivine from Greenland[19], and up to 50 R_A in kimberlite-derived 'superdeep' diamond inclusions[20] both suggest derivation from a relatively undegassed mantle. We therefore contend that the kimberlite source—and, in particular, that sampled from before 200 Ma—may represent a surviving remnant of the early mantle that has not been contaminated by extensive subduction recycling. If this is the case, then the composition recorded appears to require slightly super-chondritic Sm/Nd and Lu/Hf ratios, but with the scatter in the data encompassing values assumed in the CHUR model.

Although the primitive-kimberlite source remained very close to the CHUR model throughout its evolution, and some of the limited displacement between the two can be explained by radiogenic ingrowth alone (as even slightly non-chondritic parent/daughter-isotope ratios will lead to divergence from the CHUR model with time; see the trajectory in Fig. 2b), we have considered alternative scenarios that are capable of generating the subtle super-chondritic compositions we observe. For example, it has previously been shown that mixtures of ancient recycled basalt and sediment incorporated into the mantle may explain the present-day neodymium and hafnium isotopic compositions of ocean island basalts and MORB[21]. Following a similar reasoning, we explored the effect of subducting slab-derived materials into a primitive-mantle source. Under these scenarios, we find a best fit to the primitive-kimberlite data array is achieved by a continual 5% admixture of a slab component that is generated about 500 Myr before mixing with the mantle source region (Extended Data Fig. 1, Methods): contributions of 0–10% slab of 0.5 to 1.0 Gyr of age can be accommodated given the scatter in the data. When using higher slab/mantle ratios and/or older slab materials, calculated mixtures develop sub-chondritic hafnium-isotope values that limit involvement to relatively youthful (less than about 0.5 Gyr old) slabs. In all of these models, the preservation of linear arrays with time requires consistent slab-ageing scenarios and similar mixing proportions to be maintained throughout time and space. These experiments were conducted without any attempt to model elemental fractionation in the slab assemblage during its transit through a subduction zone, because the outcomes of this process are very poorly constrained for the lutetium–hafnium decay system. However, it is thought that subduction-zone processes will raise the Sm/Nd ratio of the slab residue[22] and thus lead to a reduction in the proportion of the slab component that could be accommodated by the primitive-kimberlite data array.

It therefore remains plausible that subduction of basaltic slabs (with or without sediment) into the deeper mantle has the potential to account for our results. However, a somewhat-restrictive set of circumstances would be required to generate the linear arrays that are defined by the kimberlite data (Fig. 1). Moreover, such a scenario does not detract from our primary conclusion, because a primordial source would be required as a starting point for any such mixing events.

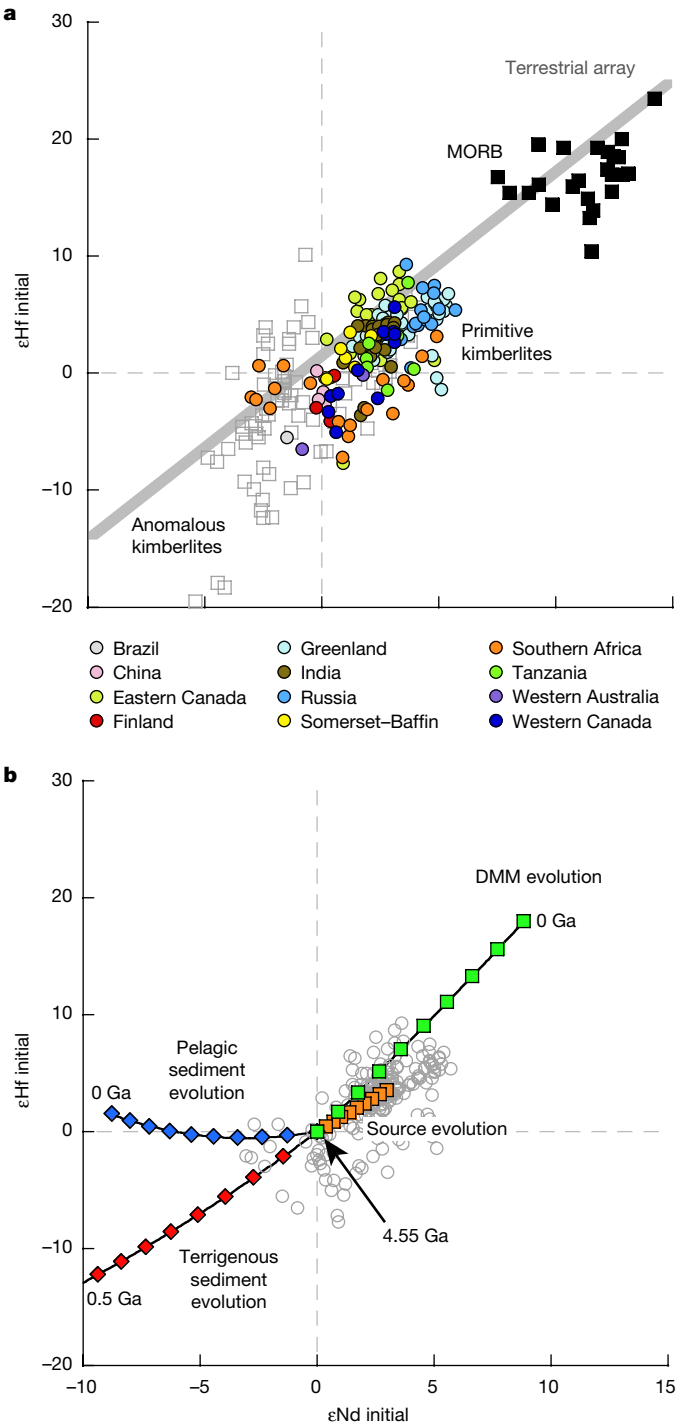

Fig. 2 | Kimberlites compared to primitive mantle. a, Initial εNd–εHf diagram, comparing the primitive (coloured circles) and anomalous (grey squares) kimberlites with the CHUR model. Symbol shapes are as for Fig. 1. Modern MORB data[10] and the terrestrial array[29] are also shown. **b**, The primitive-kimberlite array (grey circles) shown together with trajectories that illustrate the isotopic evolution of DMM, pelagic and terrigenous-sediment reservoirs from 4.55 Ga to present, in 500-Myr intervals. Much of the variability in the primitive-kimberlite array may be explained solely by radiogenic ingrowth in the source region (orange squares). The form of the array is difficult to reconcile with substantial admixtures of subducted sedimentary material.

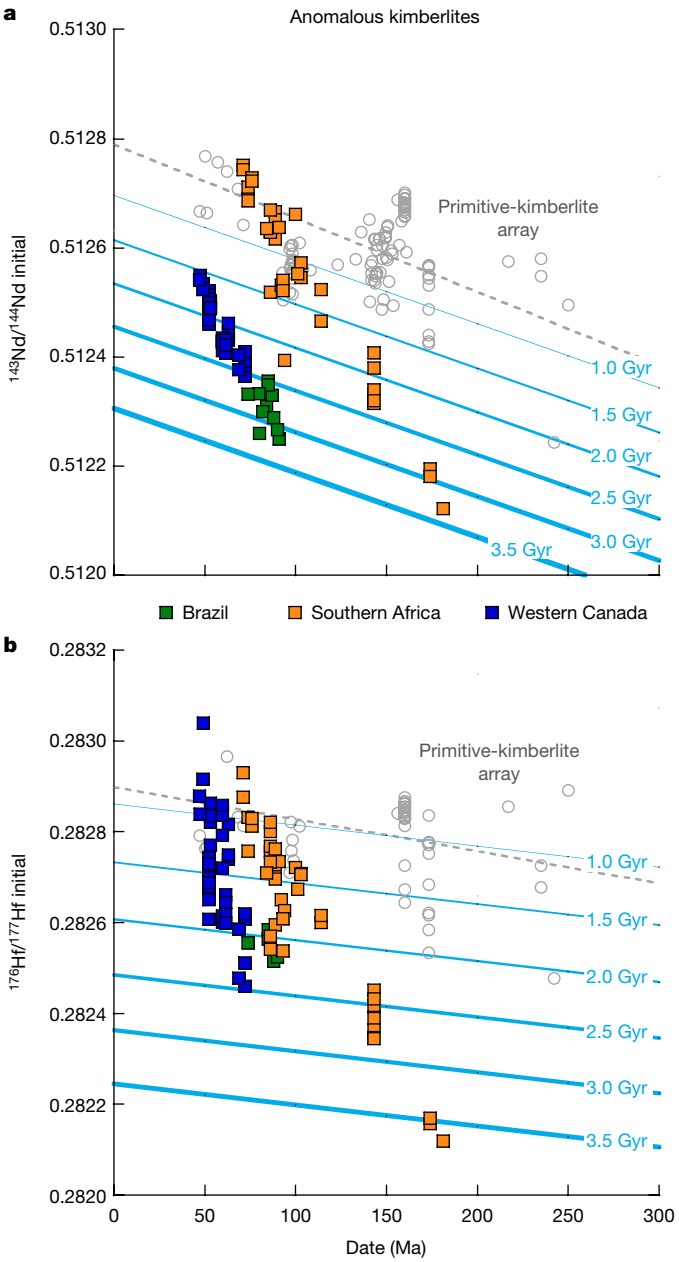

Fig. 3 | Isotopic perturbation in the anomalous kimberlites. At about 200 Ma, a major disruption is observed in kimberlites from three regions (Brazil, southern Africa and western Canada). **a**, **b**, Isotopic compositions of neodymium (**a**) and hafnium (**b**) initially fall well below the primitive-kimberlite trend (shown in grey), and then appear to evolve, very rapidly, back towards the array. Trajectories are shown (blue lines) for models of subducting slab assemblages (90% MORB and 10% terrigenous sediment), formed at different times in Earth history. Very old slabs are required to attain the isotopic shifts observed in the anomalous-kimberlite dataset.

On balance, the evolution of a single deep, isolated mantle source, with slightly super-chondritic parent/daughter-isotope ratios, offers the simplest explanation of the data and requires the least number of assumptions and special conditions. The model also best accounts for the observed high $^{3}He/^{4}He$ ratios reported for some kimberlites and diamond inclusions, and for the values of key incompatible trace-element ratios.

In the three anomalous-kimberlite suites that erupted after 200 Ma, the transition to their perturbed state appears to have been very rapid. This process occurred over a few tens of millions of years (for example, in southern Africa, the primitive Jwaneng kimberlite is dated to 235 Ma and the anomalous Silvery Home kimberlite to 181 Ma) and probably represents the effects of a single event of regional extent. At this time, the kimberlite source was substantially modified by the incorporation of a component with low $^{143}Nd/^{144}Nd$ and $^{176}Hf/^{177}Hf$ ratios (Fig. 3).

A recent study of boron-isotope variations in carbonatites worldwide[23] also shows a major isotopic and elemental perturbation around this time, towards material with an apparent influence of subduction. Global plate-tectonic reconstructions for the period that immediately precedes the development of the anomalous kimberlites (Extended Data Fig. 2) indicate that the three areas that show perturbed isotopic evolution in our dataset (Mesozoic kimberlites from southern Africa, Brazil and western Canada) are all closest to a major subduction zone along the western (Panthalassan) margin of the Pangaea supercontinent. We therefore suggest that the lowering of neodymium- and hafnium-isotope ratios at about 200 Ma may be related to subduction. A popular model for the breakup of supercontinents[24,25] involves subducting slabs, stagnating at the mantle transition zone, and then episodically avalanching into the lower mantle, which produces plume-related magmatism. As the breakup of Pangea was underway by 200 Ma, we speculate that such an avalanche may have been responsible for contaminating the post-200-Myr-old kimberlite reservoir in a manner similar to that proposed for the formation of inclusions in deeply sourced kimberlitic diamonds[26]. Modelling reveals that the isotopic departures observed in kimberlites from southern Africa and western Canada could be generated by re-activation of ancient subducting slabs (Fig. 3, Methods). However, it is important to stress that these events affected only those kimberlite sources that were close to the Panthalassan margin and that unpolluted primitive-kimberlite sources apparently still existed after 200 Ma (for example, in Tanzania or west Greenland). One further implication of our data is that the unique isotopic characteristics of some kimberlite magmas (their departure from the so-called hafnium–neodymium isotope mantle array[27]) is a relatively youthful feature, and one that is confined to a restricted group of kimberlites (the source of which was affected by a major geochemical perturbation about 200 Ma).

If the kimberlite source is representative of the composition of an early formed mantle, then the data presented here indicate that this mantle domain (at least the part that was tapped by the primitive kimberlites) remained largely isolated for much of the Earth's history, and that events around 200 Ma produced irreversible contamination of this source in at least three distinct regions. In the current dataset, signs of similar disruptive events that may have occurred before 200 Ma are difficult to detect, owing—in large part—to poor chronological constraints within suites and the sparse data for older occurrences of kimberlites. Although we cannot dismiss the possibility of earlier disruptive episodes, it is conceivable that the substantive, approximately 200-Myr-old event recorded in the global kimberlite (and carbonatite) datasets marks an important turning point in the evolution of the Earth's mantle—from a situation in which any primordial mantle(s) remained largely physically isolated to a regime in which subducting slabs penetrated into the lower mantle with much-greater regularity, as is observed at the present day[28]. These observations may therefore go some way to explaining one of the most intractable problems of the Earth's evolution; namely, the apparent paradox between present-day geophysical observations of whole-mantle convection, and geochemical arguments based upon ocean island basalts and MORB chemistry that indicate the substantive isolation of key mantle reservoirs in the past.

Online content

Any methods, additional references, Nature Research reporting summaries, source data, extended data, supplementary information, acknowledgements, peer review information; details of author contributions and competing interests; and statements of data and code availability are available at https://doi.org/10.1038/s41586-019-1574-8.

Received: 6 January 2019; Accepted: 29 July 2019;
Published online 25 September 2019.

1. Hofmann, A. W. Chemical differentiation of the Earth: the relationship between mantle, continental crust, and oceanic crust. *Earth Planet. Sci. Lett.* **90**, 297–314 (1988).
2. Hofmann, A. W. in *Treatise on Geochemistry*, 2nd edn, Vol. 3 (eds Holland, H. D. & Turekian, K. T.) 67–101 (Elsevier, 2014).
3. Jackson, M. G. et al. Evidence for the survival of the oldest terrestrial mantle reservoir. *Nature* **466**, 853–856 (2010).
4. Jackson, M. G. & Carlson, R. W. An ancient recipe for flood-basalt genesis. *Nature* **476**, 316–319 (2011).
5. Pearson, D. G. et al. Hydrous mantle transition zone indicated by ringwoodite included within diamond. *Nature* **507**, 221–224 (2014).
6. Nestola, F. et al. $CaSiO_3$ perovskite in diamond indicates the recycling of oceanic crust into the lower mantle. *Nature* **555**, 237–241 (2018).
7. Torsvik, T. H., Burke, K., Steinberger, B., Webb, S. J. & Ashwal, L. D. Diamonds sampled by plumes from the core–mantle boundary. *Nature* **466**, 352–355 (2010).
8. Henning, A., Kiviets, G., Kurszlaukis, S., Barton, E. Mayaga-Mikolo, F. Early Proterozoic metamorphosed kimberlites from Gabon. *International Kimberlite Conference: Extended Abstracts* **8**, https://doi.org/10.29173/ikc3024 (2003).
9. DePaolo, D. J. & Wasserburg, G. J. Nd isotopic variations and petrogenetic models. *Geophys. Res. Lett.* **3**, 249–252 (1976).
10. Salters, V. J. M., Mallick, S., Hart, S. R., Langmuir, C. E. & Stracke, A. Domains of depleted mantle: new evidence from hafnium and neodymium isotopes. *Geochem. Geophys. Geosyst.* **12**, Q08001 (2011).
11. Lyubetskaya, T. & Korenaga, J. Chemical composition of the Earth's primitive mantle and its variance: 1. Method and Results. *J. Geophys. Res.* **112**, B03211 (2007).
12. Palme, H. & O'Neill, H. St. C. *Treatise on Geochemistry*, 2nd edn, Vol. 3 (eds Holland, H. D. & Turekian, K. T.) 1–39 (Elsevier, 2014).
13. Trela, J. et al. The hottest lavas of the Phanerozoic and the survival of deep Archaean reservoirs. *Nat. Geosci.* **10**, 451–456 (2017).
14. Bouvier, A. & Boyet, M. Primitive Solar System materials and Earth share a common initial ^{142}Nd abundance. *Nature* **537**, 399–402 (2016).
15. Bouvier, A., Vervoort, J. D. & Patchett, P. J. The Lu-Hf and Sm-Nd isotopic composition of CHUR: constraints from unequilibrated chondrites and implications for the bulk composition of the terrestrial planets. *Earth Planet. Sci. Lett.* **273**, 48–57 (2008).
16. McDonough, W. F. & Sun, S.-S. The composition of the Earth. *Chem. Geol.* **120**, 223–253 (1995).
17. Workman, R. K. & Hart, S. R. Major and trace element composition of the depleted MORB mantle (DMM). *Earth Planet. Sci. Lett.* **231**, 53–72 (2005).
18. Rudnick, R. L. & Gao, S. in *Treatise on Geochemistry*, 2nd edn, Vol. 4 (eds Holland, H. D. & Turekian, K. T.) 1–51 (Elsevier, 2014).
19. Tachibana, Y., Kaneoka, I., Gaffney, A. & Upton, B. Ocean-island basalt-like source of kimberlite magmas from West Greenland revealed by high $^3He/^4He$ ratios. *Geology* **34**, 273–276 (2006).
20. Timmerman, S. et al. Primordial and recycled helium isotope signatures in the mantle transition zone. *Science* **365**, 692-694 (2019).
21. Chauvel, C., Lewin, E., Carpentier, M., Arndt, N. T. & Marini, J.-C. Role of recycled oceanic basalt and sediment in generating the Hf–Nd mantle array. *Nat. Geosci.* (2008).
22. Porter, K. A. & White, W. M. Deep mantle subduction flux. *Geochem. Geophys. Geosyst.* **10**, Q12016 (2009).
23. Hulett, S. R. W., Simonetti, A., Rasbury, E. T. & Hemming, N. G. Recycling of subducted crustal components into carbonatite melts revealed by boron isotopes. *Nat. Geosci.* **9**, 904–908 (2016).
24. Condie, K. C. Supercontinents and superplume events: distinguishing signals in the geologic record. *Phys. Earth Planet. Inter.* **146**, 319–332 (2004).
25. Maruyama, S., Santosh, M. & Zhao, D. Superplume, supercontinent, and post-perovskite: mantle dynamics and anti-plate tectonics on the core–mantle boundary. *Gondwana Res.* **11**, 7–37 (2007).
26. Harte, B. & Richardson, S. Mineral inclusions in diamonds track the evolution of a Mesozoic subducted slab beneath West Gondwanaland. *Gondwana Res.* **21**, 236–245 (2012).
27. Nowell, G. M. et al. Hf isotope systematics of kimberlite and their megacrysts: new constraints on their source regions. *J. Petrol.* **45**, 1583–1612 (2004).
28. van der Hilst, R. D., Widiyantoro, S. & Engdahl, E. R. Evidence for deep mantle circulation from global tomography. *Nature* **386**, 578–584 (1997).
29. Vervoort, J. D., Plank, T. & Prytulak, J. The Hf–Nd isotopic composition of marine sediments. *Geochim. Cosmochim. Acta* **75**, 5903–5926 (2011).

METHODS

Filtering the dataset. To identify subtle isotopic changes with time, our primary consideration for the inclusion of data in the compilation was that the kimberlites have robust chronological constraints. References to the relevant age determinations are provided in the Supplementary Data. Literature analyses in which ages are simply inferred were not used. We have also tried—wherever petrographic constraints allow—to limit our observations to true kimberlites and closely related rocks (largely avoiding lamproites and lamprophyres).

Kimberlite magmas are, by their very nature, susceptible to contamination during ascent and emplacement. Over the years, a variety of methods have been developed to filter geochemical datasets to circumvent these effects. These methods range from simple petrographic observations through to more-sophisticated geochemical approaches, such as the Clement contamination index ($CCI = [(SiO_2 + Al_2O_3 + Na_2O)/(MgO + 2K_2O)]$)[30] and other methods that use geochemistry[31,32]. Unfortunately, none of these is universally applicable because the contaminants vary considerably from site to site. For the literature data compiled as part of this study, we generally relied on the assessments of the authors themselves as to which samples may have been influenced by contamination.

For our own samples, where major-element analyses were available we have adopted a minimalist approach and excluded only data with $CCI > 1.5$ (excluded data are labelled in the Source Data) as a precaution—although we note that no correlations can be observed between CCI and isotopic compositions, even if these data are included. In the case of the Lac De Gras kimberlites, it was previously observed[31] that the CCI does not provide a sensitive tracer of crustal contamination because the addition of crust and mantle produce opposing effects on the CCI index. The authors of this previous study therefore adopt a more-rigorous filter that uses bulk aluminium or ytterbium, or ln(Si/Al) versus ln(Mg/Yb). To provide consistency, we have adopted the same filter for our own data from Lac de Gras kimberlites.

We excluded one kimberlite occurrence in its entirety from the literature compilation; the Triassic–Jurassic kimberlites from eastern North America[33].These kimberlites show age-progressive volcanism, and appear to have a genetic association with the Great Meteor hotspot track: as such we do not consider them to be representative of the global kimberlite source reservoir.

Major- and trace-element analyses. For major-element analysis, samples were prepared as fused glass discs using a mixed lithium metaborate/tetraborate flux and analysed on a SPECTRO Xepos energy dispersive XRF spectrometer in the School of Earth Sciences (University of Melbourne). Calibrations were constructed using a wide variety of internationally recognized certified reference materials, and analyses of secondary reference materials suggest an accuracy of generally better than 1–2% for most elements. Analytical reproducibility is generally better than 1% for most elements, with the exception of P_2O_5 (up to 2%) and Na_2O (up to 4%).

For trace-element analysis of samples analysed at the University of Melbourne, agate-milled powders were dissolved at high pressure in 'Parr-style' dissolution vessels overnight at 150 °C, and then refluxed with nitric acid to remove fluorides. Analytical and drift correction procedures follow a previous publication[34], using a natural rock standard for calibration, internal drift correction using multi-internal standards (^{6}Li, ^{84}Sr, Rh, ^{147}Sm, rhenium and ^{235}U), external drift monitors and aggressive washout procedures. Differences from the previously described[34] protocol include: (1) thulium, indium and bismuth were not used as internal standards because they are measured as analytes; and (2) two digestions of the US Geological Survey (USGS) standard W-2 are used for instrument calibration. Samples were analysed on an Agilent 7700x instrument. The instrument was tuned to provide cerium oxide levels of <1%. Four replicates of 100 scans per replicate were measured for each isotope. Dwell times were 10 ms, except for beryllium, cadmium, indium, antimony, tantalum, tungsten, thalium and bismuth, for which dwell times were 30 ms. Long sample wash-out times of 6 min with solutions of 0.5% Triton X-100, 0.025% HF in 5% HNO_3 and 2% HNO_3 and long sample-uptake times of 120 s were used.

Trace-element data used for age correction of kimberlite neodymium- and hafnium-isotope ratios (from Durham University) were determined on a Perkin Elmer Sciex Elan 6000 inductively coupled plasma mass spectrometry (ICP-MS) instrument using previously outlined techniques[35]. Seven repeat dissolutions of an in-house kimberlite standard K2WI yielded Sm/Nd and Lu/Hf reproducibility of 1.1% and 2.4%, respectively.

Neodymium and hafnium isotope ratios. The majority of new isotope-ratio analyses presented here were obtained at the University of Melbourne, after sequential extraction of hafnium and neodymium[36,37], following standard dissolution procedures. We note that although zircons sometimes occur in kimberlites as megacrysts, their abundance is considerably less than even that of diamond; that is, a low ppm by volume. As a result, the chances of incorporating the typically centimetre-sized zircon megacrysts into our samples during powdering, and dissolution is essentially zero. Furthermore, a number of studies have now demonstrated that zircons[27] (and indeed other members of the megacryst suite) exhibit the same hafnium-isotopic compositions as the kimberlites that entrain them. Therefore, even in the highly unlikely event that rare fragments of zircon were entrained but not dissolved, the composition that we measured would be indistinguishable from the bulk rock–zircon mix.

Isotopic compositions were measured on a Nu Plasma multi-collector ICP-MS. Instrumental mass bias was corrected by internal normalization to $^{146}Nd/^{144}Nd = 0.7219$ and $^{179}Hf/^{177}Hf = 0.7325$ using the exponential law, and $^{143}Nd/^{144}Nd$ and $^{176}Hf/^{177}Hf$ are reported relative to La Jolla neodymium (0.511860) and JMC475 hafnium (0.282160), respectively. External precisions (2 s.d.) are ±0.000020 and ±0.000015, respectively, based on results for rock standards. Neodymium- and hafnium-isotope data for BCR-2 were acquired simultaneously, with the kimberlite dataset average of 0.512637 ± 13 (±2 s.d., $n = 4$) and 0.282866 ± 16 (±2 s.d., $n = 5$), consistent with reference values[38]. Sm/Nd and Lu/Hf ratios for age corrections were calculated from high-precision trace-element data obtained by quadrupole ICP-MS for a split of each sample solution; external precisions on $^{147}Sm/^{144}Nd$ and $^{176}Lu/^{177}Hf$ are ±2%, and duplicate analyses on a small dataset by isotope dilution methods suggest an accuracy of better than 2% for samarium and neodymium, and 3% for lutetium and hafnium. Monte Carlo simulations suggest that these uncertainties are a very minor component of the overall uncertainty budget in age-corrected epsilon values, which are dominated by the measurement uncertainty on the isotope ratio. In cases in which reliable whole-rock samples were unavailable (for example, for Tanzania), perovskite data have been used. These were obtained by procedures similar to those documented above.

Data for the western Canada kimberlites were obtained at the NERC Isotope Geosciences Laboratory (NIGL; Keyworth) and Durham University. Full details of the dissolution and sequential extraction of hafnium and neodymium have previously been published[39]. In brief, 100mg of agate-milled powder was dissolved in concentrated HF–HNO_3 at 120 °C for 3 days, followed by repeat dry-downs in concentrated HNO_3 and then 6 M HCl to break down fluorides.

Following dissolution, a cation-exchange resin column was used to collect hafnium and rare-earth-element (REE) fractions. Neodymium was analysed on the REE fraction without further processing to remove samarium. The hafnium fraction was processed through a second anion-exchange column to remove titanium before analysis. The majority of samples were analysed for both hafnium- and neodymium-isotopic composition on a Neptune multi-collector ICP-MS at Durham University; a small subset of samples (identified in the Source Data) were analysed for neodymium on a MAT-262 thermal ionization mass spectrometer (TIMS), and for hafnium on a P54 multi-collector ICP-MS at NIGL. Those samples analysed for neodymium isotopes by TIMS at NIGL were further processed through HDEHP columns to obtain a samarium-free pure neodymium fraction.

For neodymium analysis by MAT-262 TIMS, instrumental mass bias was corrected using a $^{146}Nd/^{144}Nd$ ratio of 0.7219 and an exponential law. For Nd analysed on the Neptune instrument, mass bias was corrected using a $^{146}Nd/^{145}Nd$ ratio of 2.079143 (equivalent to a $^{146}Nd/^{144}Nd$ ratio of 0.7219). The $^{146}Nd/^{145}Nd$ ratio was used because neodymium was measured on a total REE-cut from the first cation-column stage, and this is the only cerium- and samarium-free stable neodymium-isotope ratio. This approach obviously requires a correction for isobaric interferences from samarium on ^{144}Nd, ^{148}Nd and ^{150}Nd, and has previously been described[40]. The accuracy of the samarium-correction method during analysis of a total REE fraction is demonstrated by repeat analyses of BHVO-1, which provided an average $^{143}Nd/^{144}Nd$ ratio of 0.512982 ± 0.000007 (13.5 ppm, ± 2 s.d., $n = 13$) after the samarium correction; this was identical to the TIMS ratio of 0.512986 ± 0.000009 (17.5 ppm, ± 2 s.d., $n = 19$) based on purified neodymium cuts[41].

For hafnium-isotope analysis on the P54 and Neptune instruments, instrumental mass bias was corrected using a $^{179}Hf/^{177}Hf$ ratio of 0.7325. The hafnium-isotope composition of BHVO-1 analysed on the same dissolutions on which neodymium data were obtained yielded an average $^{176}Hf/^{177}Hf$ of 0.283104 ± 0.000008 (28.3 ppm, ±2 s.d., $n = 13$), identical to reference values[41]. All $^{143}Nd/^{144}Nd$ and $^{176}Hf/^{177}Hf$ ratios for kimberlites from western Canada are reported relative to La Jolla neodymium (0.511860) and JMC475 hafnium (0.282160), respectively. External precisions (±2 s.d.) for data obtained at Durham University are better than ±0.000018 (including analysis of pure and samarium-doped J & M isotope reference material) and ±0.000012, respectively, and for data obtained at NIGL are ±0.000019 and ±0.000012, respectively (based on repeat analysis of isotope reference materials J & M and JMC475 during each analytical session).

εNd and εHf values were calculated using previously published chondrite compositions[15]. The half-lives of ^{147}Sm and ^{176}Lu used are 6.54×10^{-12} per year and 1.867×10^{-11} per year, respectively.

Geochronology. For the majority of samples, age determinations from the literature have been used, and these are noted in the Source Data. For the Silvery Home kimberlite, a phlogopite rubidium–strontium age was determined. Phlogopite samples were washed in hot water, spiked with an ^{85}Rb–^{84}Sr tracer and dissolved on a hotplate. Strontium was extracted and purified using two passes over small

(0.15-ml) beds of Eichrom strontium resin (50–100 mm), which reduced rubidium and $BaAr^{++}$ interference during strontium-isotope analyses on the MC-ICP-MS to negligible levels. Rubidium was purified using cation exchange and analysed using zirconium doping. Data for a single unleached phlogopite fraction from Silvery Home yields a relatively low Rb/Sr ratio and $^{87}Sr/^{86}Sr$ ratio. Combined with data for perovskite[42], the phlogopite provides a two-point rubidium–strontium age of 181.3 ± 1.6 Myr, which is consistent with—but more precise than—the laser ablation ICP-MS uranium–lead age for perovskite of 183 ± 35 Myr[43] (Extended Data Table 1).

Modelling alternative scenarios for generating the primitive-kimberlite array. Two processes were explored as a means of generating the primitive-kimberlite data arrays through time (Fig. 1) and the deviations from CHUR (Fig. 2); Extended Data Table 2 provides the modelling parameters.

In the first process, we used the best-fit lines (through somewhat-scattered data) anchored to the CHUR model at 4.55 Ga in Fig. 1 to provide an estimate of the present-day neodymium- and hafnium-isotope compositions of the primitive-mantle source, and thus the parent/daughter-isotope ratios required for the evolution of this source. Because these parent/daughter-isotope ratios differ slightly from the CHUR model, isotopic compositions will necessarily depart from the CHUR model with time; a trajectory included in Fig. 2 illustrates this effect (that is, the isotopic variation that can be expected in this reservoir from radiogenic ingrowth alone). We note that—although the scatter in the measured data does not preserve a strict age progression (not shown)—radiogenic evolution of this modelled source alone would generate 4–5 epsilon units of scatter (half of the scatter that was observed) without recourse to any open-system processes such as mixing.

In the second model, we simulated the incorporation of subducted slabs into a CHUR-like lower-mantle source region, from which kimberlite melts were then produced. We ran numerous models that allowed the N-MORB component to age by between 0 and 2 Gyr before a mixing of between 0 and 15% slab component into the primitive-mantle source. Although the scatter in the data can accommodate the addition of between 0–10% of a 0.5–1-Gyr-old slab at the time of mixing, the model arrays that most-closely approximate the data in Fig. 1 were generated by the continuous addition of 5% slab component (predominantly basalt, although minor sedimentary components have little effect at such low levels of slab involvement) that was 500 Myr old at the time of mixing into 95% CHUR, followed by the generation of kimberlite magmas (Extended Data Fig. 1). Although this mixing model was arithmetically achievable, it still requires a deep-mantle reservoir with primordial compositional characteristics to provide most of the material input.

Modelling the origins for the anomalous-kimberlite arrays. The anomalous post-200-Myr-old kimberlite source is marked by a sudden departure from the main primitive-kimberlite evolutionary trend, followed by a relatively rapid track back towards this array (Fig. 3).

Although crustal contamination has the potential to shift neodymium- and hafnium-isotope ratios to lower values, it is hard to envisage any scenario in which such processes would be suddenly initiated in 3 widely dispersed continental locations at about 200 and 100 Ma (Fig. 3). Furthermore, the linear arrays evolving with time back towards the mantle array would require a highly systematic control, whereas crustal contamination is usually seen as a more random process and zircon megacrysts—which have not experienced any upper-level crustal contamination—show very similar time–composition relationships[44]. Finally, any kimberlite that experienced such extreme levels of crustal contamination would no longer retain its primary magmatic characteristics. For all these reasons, and because samples have been filtered for crustal-contamination effects, we consider crustal contamination an unlikely scenario for generating these arrays.

The geographical arrangement of these sites (Extended Data Fig. 2) suggests a possible link with palaeo-subduction events, and it is accepted that subducted slab signatures can produce the general form of the neodymium–hafnium mantle array[21]. A number of these anomalous kimberlites from southern Africa, Brazil and western Canada also exhibit increased strontium-isotope ratios with $^{87}Sr/^{86}Sr$ up to 0.706, which further suggests an influence of subduction[42,45]. We have proposed that subducted slabs ponding at the transition zone and, eventually (around 200 Ma), avalanching into the lower mantle may have triggered these departures from the primitive-kimberlite evolutionary trend by the incorporation of ancient subduction components. We further explore two aspects of this hypothesis: first, the processes required to attain these unusual isotopic shifts and second, the nature of the steep linear arrays observed in time versus compositional space.

The origin of the enriched isotopic signatures. The unusual departures from the mantle array seen in the post-200-Myr-old kimberlites from southern Africa, western Canada and Brazil require ancient sources with a protracted history of evolution under sub-chondritic parent/daughter-ion ratios. Following a previous approach[21], we modelled the likely effect of subducting ancient slabs (basalt plus sediment) into the deep mantle and storing them there to be tapped by post-200-Myr-old kimberlite magmatism.

Using a conservative mixture of 90% MORB/10% sediment in the subducting slab assemblage, we find that the first expression of both the southern African and western Canada anomalous kimberlites (that is, those with the most substantial departure from the mantle array) could be generated from ancient slabs subducted into the mantle (Fig. 3), but that these would have to be around 3–3.5 Gyr old to accommodate the large isotopic shifts observed—at least with the parameters used in our study. These represent minimum values, as our calculation does not consider the effects of subsequent mantle mixing (which would shift compositions to more-radiogenic values). We find that terrestrial sediments provide a better fit than pelagic sediments in such a model: pelagic sediments can be used, but require a larger proportion of sediment or an older slab. At present, the Brazil array is insufficiently well-characterized to enable a similar calculation. Ultimately, metasomatic processes—linked to subduction—may provide a more-tractable solution to this problem, but investigation of such phenomena is beyond the scope of this study.

The origin of the linear arrays with time. The steep linear trends observed with time in these three kimberlite suites suggest a very well-defined chemical evolution. Perhaps the most-obvious way of achieving this would be to mix the slab component with a depleted asthenospheric mantle upon eruption: in Extended Data Fig. 3, we explore this possibility. For simplicity, we ignore prior mixing with primitive mantle in this calculation and focus entirely on mixing slab components with depleted upper mantle on kimberlite ascent. Kimberlite melts of any given age must mix with DMM of the same age and, as a result, all mixing vectors are vertical in this diagram. As such, any constant proportion of DMM entrainment will not produce the steep arrays noted in anomalous-kimberlite data. The only way to generate arrays such as these would be by the progressive and substantial increase in the DMM component with successive magmatic episodes (vertical displacement), which would have to also somehow be highly correlated with the age of mixing (horizontal displacement). Such a process seems unlikely, as the trace-element compositions of the kimberlites do not change through time and the same process would have to be mirrored on three continents. Similar vectors are obtained by mixing with primitive, rather than depleted, mantle.

Because mixing does not appear to be able to generate the steep trends observed in the kimberlite data, a second possibility is that radiogenic ingrowth within the source itself could account for the sub-parallel trends observed—indeed, we previously invoked a similar model for the genesis of steep time–composition relationships observed in the zircon megacrysts[44] that are found in some kimberlites. However, it is important to note that such radiogenic ingrowth would require highly elevated parent/daughter-isotope ratios in the source (in the case of the southern Africa dataset, these are a $^{176}Lu/^{177}Hf$ ratio of 0.326 and $^{147}Sm/^{144}Nd$ ratio of 0.78, and in the case of western Canada, even-more-extreme values of 0.963 and 1.07 for the $^{176}Lu/^{177}Hf$ ratio and $^{147}Sm/^{144}Nd$ ratio, respectively). Ratios such as these could be attained only under the influence of garnet, and would therefore impose strong constraints on the maximum depth of the source rocks—and perhaps involve carbonatite metasomatism to produce highly increased parent/daughter-ion ratios at the outset[43].

Data availability

All data generated or analysed during the course of this study are archived at EarthChem (https://doi.org/10.1594/IEDA/111335).

30. Clement, C. R. A comparative geological study of some major kimberlite pipes in Northern Cape and Orange Free State. PhD thesis, Univ. of Cape Town (1982).
31. Kjarsgaard, B. A., Pearson, D. G., Tappe, S., Nowell, G. M. & Dowall, D. P. Geochemistry of hypabyssal kimberlites from Lac de Gras, Canada: comparisons to a global database and applications to the parent magma problem. *Lithos* **112**, 236–248 (2009).
32. Le Roex, A. P., Bell, D. R. & Davis, P. Petrogenesis of group I kimberlites from Kimberley, South Africa: evidence from bulk rock geochemistry. *J. Petrol.* **44**, 2261–2286 (2003).
33. Heaman, L. M. & Kjarsgaard, B. A. Timing of eastern North American kimberlite magmatism: continental extension of the Great Meteor hotspot track? *Earth Planet. Sci. Lett.* **178**, 253–268 (2000).
34. Eggins, S. M. et al. A simple method for the precise determination of ≥40 trace elements in geological samples by ICPMS using enriched isotope internal standardisation. *Chem. Geol.* **134**, 311–326 (1997).
35. Ottley, C. J., Pearson, D. G. & Irvine, G. J. in *Plasma Source Mass Spectrometry – Applications and Emerging Technologies* (eds Holland, G. & Tanner, S. D.) 221–230 (Royal Society of Chemistry 2003).
36. Münker, C., Weyer, S., Scherer, E. & Mezger, K. Separation of high field strength elements (Nb, Ta, Zr, Hf) and Lu from rock samples for MC-ICPMS measurements. *Geochem. Geophys. Geosyst.* **2**, 1064 (2001).
37. Pin, C. & Santos-Zalduegui, J. F. Sequential separation of light rare-earth elements, thorium and uranium by miniaturized extraction chromatography: application to isotopic analyses of silicate rocks. *Anal. Chim. Acta* **339**, 79–89 (1997).

38. Jweda, J., Bolge, L., Class, C. & Goldstein, S. L. High precision Sr-Nd-Hf-Pb isotopic compositions of USGS reference material BCR-2. *Geostand. Geoanal. Res.* **40**, 101–115 (2016).
39. Dowall, D. P., Nowell, G. M. & Pearson, D. G. in *Plasma Source Mass Spectrometry – Applications and Emerging Technologies* (eds Holland, G. & Tanner, S. D.) 321–337 (Royal Society of Chemistry, 2003).
40. Nowell, G. M. & Parrish, R. R. in *Plasma Source Mass Spectrometry: the New Millennium* (eds Holland, J. G. & Tanner, S. D.) 298–310 (Royal Society of Chemistry, 2001).
41. Weis, D., Kieffer, B., Maerschalk, C., Pretorius, W. & Barling, J. High-precision Pb-Sr-Nd-Hf isotopic characterization of USGS BHVO-1 and BHVO-2 reference materials. *Geochem. Geophys. Geosyst.* **6**, Q02002 (2005).
42. Woodhead, J., Hergt, J., Phillips, D. & Paton, C. African kimberlites revisited: in situ Sr-isotope analysis of groundmass perovskite. *Lithos* **112**, 311–317 (2009).
43. Griffin, W. L. et al. Emplacement ages and sources of kimberlites and related rocks in southern Africa: U-Pb ages and Sr-Nd isotopes of groundmass perovskite. *Contrib. Mineral. Petrol.* **168**, 1032 (2014).
44. Woodhead, J., Hergt, J., Giuliani, A., Phillips, D. & Maas, R. Tracking continental-scale modification of the Earth's mantle using zircon megacrysts. *Geochem. Perspect. Lett.* **4**, 1727 (2017).
45. Tappe, S., Pearson, D. G., Kjarsgaard, B. A., Nowell, G. & Dowall, D. Mantle transition zone input to kimberlite magmatism near a subduction zone: origin of anomalous Nd–Hf systematics at Western Canada, Canada. *Earth Planet. Sci. Lett.* **371–372**, 235–251 (2013).
46. Odin, D.S. et al. in *Numerical Dating in Stratigraphy* Part 1 (ed. Odin, G. S.) 123–148 (John Wiley & Sons, 1982).
47. Gale, A., Dalton, C. A., Langmuir, C. H., Su, Y. & Schilling, J.-G. The mean composition of ocean ridge basalts. *Geochem. Geophys. Geosyst.* **14**, 489–518 (2013).
48. Vervoort, J. D. & Blichert-Toft, J. Evolution of the depleted mantle: Hf isotope evidence from juvenile rocks through time. *Geochim. Cosmochim. Acta* **63**, 533–556 (1999).
49. Chauvel, C. et al. Constraints from loess on the Hf–Nd isotopic composition of the upper continental crust. *Earth Planet. Sci. Lett.* **388**, 48–58 (2014).
50. Scherer, E., Munker, C. & Mezger, K. Calibration of the lutetium–hafnium clock. *Science* **293**, 683–687 (2001).
51. Söderlund, U., Patchett, P. J., Vervoort, J. D. & Isachsen, C. E. The ^{176}Lu decay constant determined by Lu–Hf and U–Pb isotope systematics of Precambrian mafic intrusions. *Earth Planet. Sci. Lett.* **219**, 311–324 (2004).
52. Lugmair, G. W. & Marti, K. Lunar initial ^{143}Nd/^{144}Nd: differential evolution of the lunar crust and mantle. *Earth Planet. Sci. Lett.* **39**, 349–357 (1978).
53. Scotese, C. R. *PALEOMAP PaleoAtlas for GPlates and the PaleoData Plotter* http://www.earthbyte.org/paleomap-paleoatlas-for-gplates/ (2016).
54. Müller, R. D. et al. Ocean basin evolution and global-scale plate reorganization events since Pangea breakup. *Annu. Rev. Earth Planet. Sci.* **44**, 107–138 (2016).

Acknowledgements We thank the De Beers Group, S. Graham, B. Kjarsgaard and H. O'Brien for access to samples; M. Felgate and A Greig for technical assistance; D. Sandiford for advice on the use of GPlates; and S. Shirey for suggestions. R. Chesler and M. Felgate produced the Tanzania perovskite and Brazilian kimberlite data, respectively. J.W. and A.G. acknowledge funding from the Australian Research Council.

Author contributions J.W., R.M. and G.N. were responsible for the acquisition of new isotope data. J.H. and A.G. collated existing data. J.W., J.H. and A.G. conducted the data analysis. D.P. and D.G.P. contributed to geochemical and geological interpretations, sample selection and sample screening. All authors contributed to writing the paper.

Competing interests The authors declare no competing interests.

Additional information
Supplementary information is available for this paper at https://doi.org/10.1038/s41586-019-1574-8.
Correspondence and requests for materials should be addressed to J.W.
Peer review information *Nature* thanks Catherine Chauvel, Alex Sobolev and Richard J. Walker for their contribution to the peer review of this work.
Reprints and permissions information is available at http://www.nature.com/reprints.

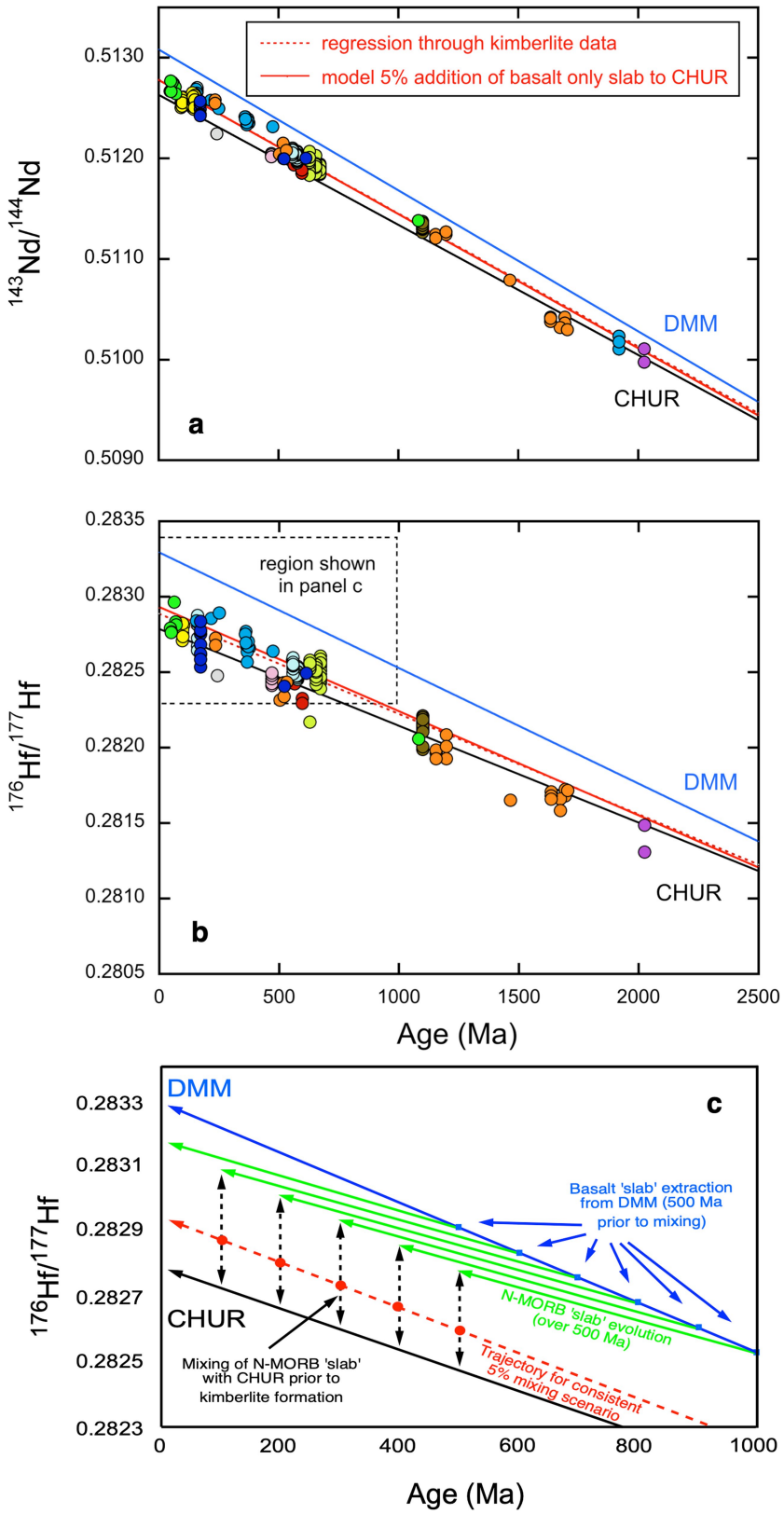

Extended Data Fig. 1 | A model for generating the primitive-kimberlite array. a, **b**, Model simulating the neodymium- (**a**) and hafnium- (**b**) isotope variations generated by the incorporation of subducted slab (normal MORB (N-MORB), plus 0–5% sediment) into a CHUR-like lower-mantle source region from which kimberlite melts are produced. **c**, The best fit to the observed data is achieved via the continuous addition (black arrows) of a 5% slab component (here, N-MORB) that has been allowed to age by 500 Myr (green arrows) before mixing with the CHUR source (95% in **c**). Evolution trajectories similar to the green arrows for N-MORB are generated in the model when incorporating a sedimentary component (which, for clarity, is not shown). The addition of 95% of a deep-mantle reservoir with primitive-mantle compositional characteristics would still be required as a starting point for each mixing step.

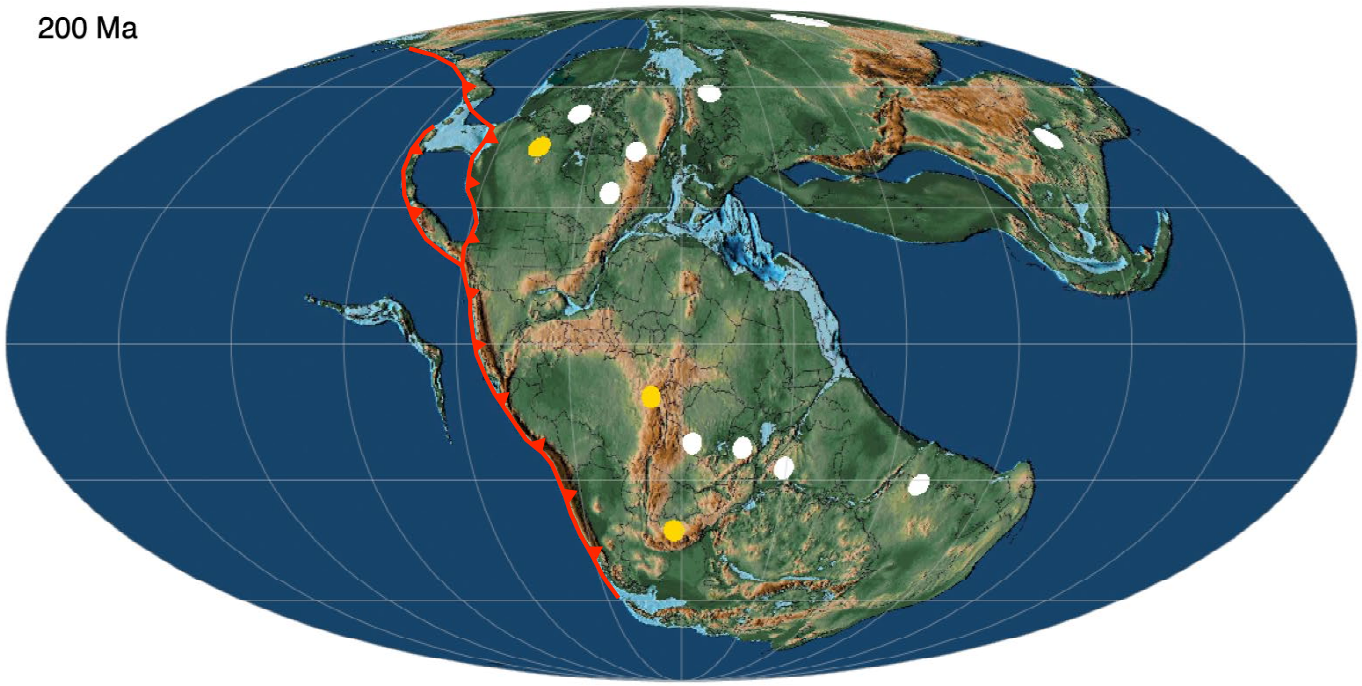

Extended Data Fig. 2 | Reconstructions of the Pangea supercontinent at 200 Ma. Figure produced using PALEOMAP[53] and GPlates 2.0. White circles provide indicative locations for primitive kimberlites, and gold circles indicate anomalous-kimberlite localities. Red lines indicate subduction zones at the western edge of Pangea[54].

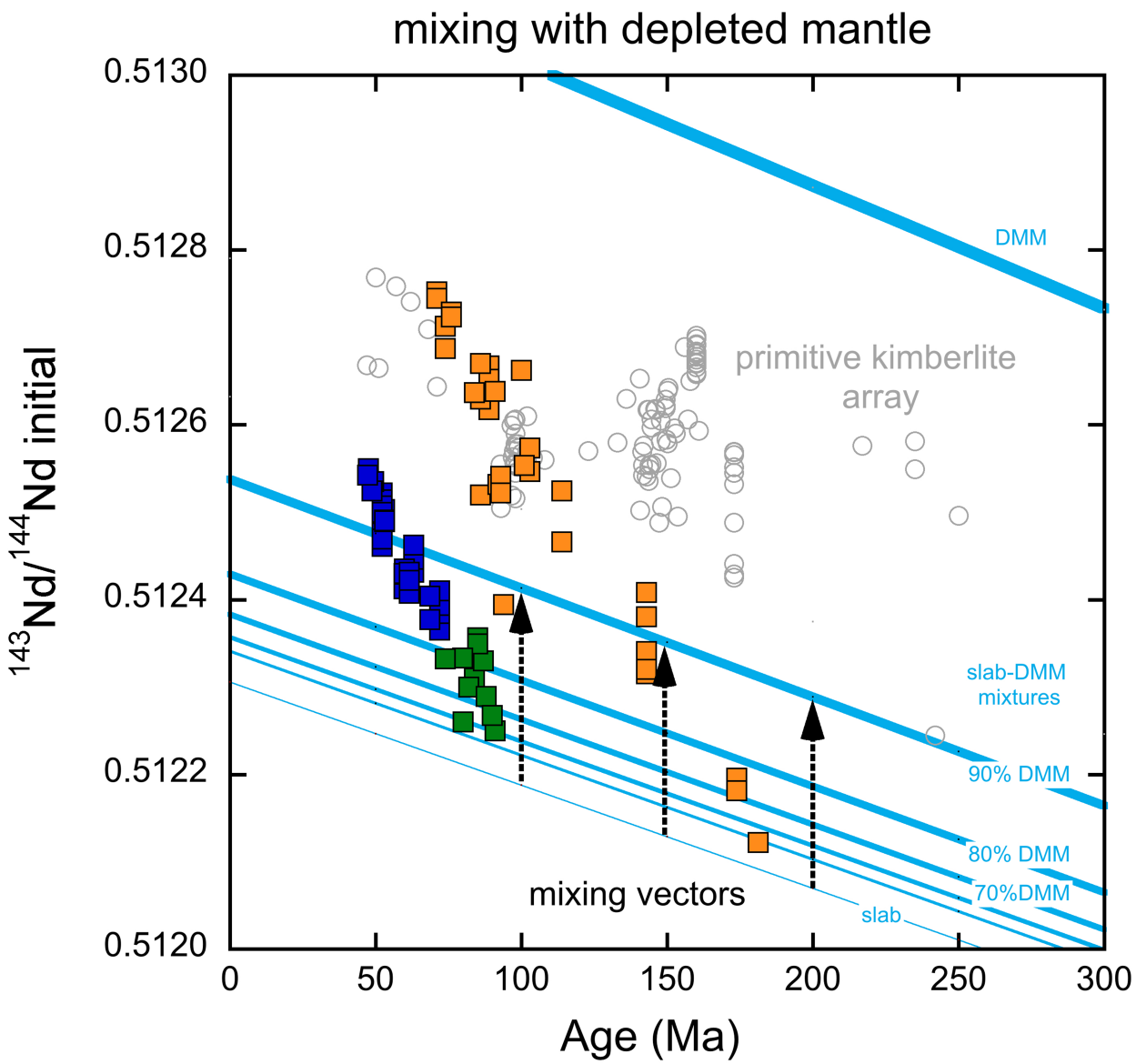

Extended Data Fig. 3 | Subducted slab-DMM mixing arrays in relation to the anomalous-kimberlite data. Although assimilation of DMM by an ascending enriched 'kimberlite' component might be considered the most obvious way of generating the steep data arrays in the anomalous kimberlites, melts of any given age must mix with DMM of the same age. Thus, mixing vectors do not point towards modern DMM; they are vertical in age versus the isotope-ratio diagrams. Consequently, any constant proportion of DMM entrainment will not produce the steep arrays noted in the anomalous-kimberlite data. Instead, a progressive and substantial increase in the DMM component with successive magmatic episodes (vertical displacement) would be required—which would also have to be highly correlated with the age of mixing (horizontal displacement). Similar vectors are obtained by mixing with primitive, rather than depleted, mantle.

Extended Data Table 1 | Isotope data used to generate an age for the Silvery Home kimberlite

Sample	Rb_{ppm}	Sr_{ppm}	$^{87}Rb/^{86}Sr$	$^{87}Sr/^{86}Sr$	2se
#24 phlogopite	318.4	173.1	5.328	0.720071	0.000017
Perovskite[42]				0.706580	0.000127

Reference material	Rb_{ppm}	Sr_{ppm}	$^{87}Rb/^{86}Sr$	$^{87}Sr/^{86}Sr$	model age* (Ma)
standard Glauconite, GLO-1 (90.4 Ma, Odin et al.[46])					
GLO-1	228.8	18.21	36.506	0.753630	90.7±0.5
GLO-1	231.0	18.32	36.626	0.753595	90.4±0.5

Standard glauconite reference material (GLO-1) was taken from a previous publication[46]. Mass bias in strontium-isotope runs corrected by internal normalization to an $^{88}Sr/^{86}Sr$ ratio of 8.37521, using the exponential law. The $^{87}Sr/^{86}Sr$ ratio is reported relative to SRM 987 (0.710230), and has an external precision of ±0.000040 (±2 s.d.). The mass bias in spiked rubidium runs was corrected by normalization to a $^{90}Zr/^{91}Zr$ ratio of 4.584514 in dopant zirconium. The $^{87}Rb/^{86}Sr$ ratio was obtained by isotope dilution, and has an external precision of ±0.5% (±2 s.d.).
*Model ages for GLO-1 were calculated with an initial $^{87}Sr/^{86}Sr$ ratio of 0.7074.

Extended Data Table 2 | Modelling parameters used in this study

Reservoir	Sm_{ppm}	Nd_{ppm}	$^{147}Sm/^{144}Nd$	$^{143}Nd/^{144}Nd$	Lu_{ppm}	Hf_{ppm}	$^{176}Lu/^{177}Hf$	$^{176}Hf/^{177}Hf$	Reference
CHUR (present)	-	-	0.196	0.512630	-	-	0.0336	0.282785	15
PM	0.4347	1.341	-	-	0.07083	0.3014	-	-	12
N-MORB	3.48	10.66	-	-	0.48	2.46	-	-	47
DMM	0.239	0.581	-	-	0.058	0.157	-	-	17
	-	-	-	-	-	-	-	0.283294	48
	-	-	-	0.513083	-	-	-	-	47
Terrigenous sediment			0.1193	0.512101	-	-	0.0125	0.282412	49
	4.7	27	-	-	0.31	5.3	-	-	18
Pelagic sediment	5.78	27	0.1296	0.51218	0.413	4.06	0.0142	0.282829	21

Decay constants	$\lambda^{176}Lu$ = 1.867 e-11 (refs 50,51), $\lambda^{147}Sm$ = 6.54 e-12 (ref. 52)

Data pertaining to reservoir materials[12,15,17,18,21,47–49] and the decay constants[50–52] were taken from previous publications.